

A hemisphere array for non-invasive ultrasound brain therapy and surgery

G T Clement, Jie Sun, Tonia Giesecke and Kullervo Hynynen

Department of Radiology, Brigham and Women's Hospital, Harvard Medical School, Boston, MA 02115, USA

Received 14 June 2000, in final form 18 August 2000

Abstract. Ultrasound phased arrays may offer a method for non-invasive deep brain surgery through the skull. In this study a hemispherical phased array system is developed to test the feasibility of trans-skull surgery. The hemispherical shape is incorporated to maximize the penetration area on the skull surface, thus minimizing unwanted heating. Simulations of a 15 cm radius hemisphere divided into 11, 64, 228 and 512 elements are presented. It is determined that 64 elements are sufficient for correcting scattering and reflection caused by trans-skull propagation. An optimal operating frequency near 0.7 MHz is chosen for the array from numerical and experimental thermal gain measurements comparing the power between the transducer focus and the skull surface. A 0.665 MHz air-backed PZT array is constructed and evaluated. The array is used to focus ultrasound through an *ex vivo* human skull and the resulting fields are measured before and after phase correction of the transducer elements. Finally, to demonstrate the feasibility of trans-skull therapy, thermally induced lesions are produced through a human skull in fresh tissue placed at the ultrasound focus inside the skull.

(Some figures in this article are in colour only in the electronic version; see www.iop.org)

1. Introduction

Brain tumours and other disorders of the brain could benefit from non-invasive surgery using ultrasound (Robinson and Lele 1972, Fry *et al* 1986, Hynynen *et al* 1997). Similar to other therapeutic ultrasound procedures, an intense focused pressure field can be produced to destroy tissue by coagulative necrosis. However, non-invasive treatment in the brain requires propagation through the skull bone, which generally destroys a focused wave (Fry and Goss 1980).

While other techniques for propagation of transcranial ultrasound have been investigated (Fry 1977, Fry and Goss 1980, Tanter *et al* 1998), element phasing has recently been shown to be an effective method for correcting distortion caused by the skull (Hynynen and Jolesz 1998). Previous simulations (Sun and Hynynen 1998) and experiments (Hynynen and Jolesz 1998, Clement *et al* 2000) have demonstrated that ultrasound can be focused in precise regions in the brain if the phase distortions introduced by the skull are corrected by proper element phasing. However, in addition to focusing energy, heating outside the region of treatment must be avoided (Sun and Hynynen 1999). This is a particular concern on the skull surface where both reflection and attenuation coefficients are high. Our approach to this problem is a large hemispherical array design, which surrounds the top of the head and thus distributes the energy over a large area of the skull surface. In the current study a practical array is designed, constructed and tested to assess the practical feasibility of the therapy.

2. Methods

2.1. Simulation

Simulations of the acoustic pressure field propagated through the skull and into the brain were performed using the previously described method by Sun and Hynynen (1998). The algorithm was implemented by dividing the ultrasound propagation path into a series of layers which allows successive application of a discrete approximation to the Rayleigh surface integral:

$$p = \sum_{i_1}^{N_1} \dots \sum_{i_M}^{N_M} \prod_{l=1}^{M-1} \left[\frac{ik_{c_l}}{2\pi} \frac{e^{-ik_{c_l} R_{i_l, i_{l+1}}}}{R_{i_l, i_{l+1}}} \left(1 - i \frac{1}{k_{c_l} R_{i_l, i_{l+1}}} \right) T_{v_{l+1}} \cos(\theta_{i_{l+1}, t}) \right] \times \left(\frac{ik_{c_M} \rho_M c_M}{2\pi} \frac{e^{-ik_{c_M} R_{i_M}}}{R_{i_M}} \right) u_{i_1} \left(\prod_{l=1}^M ds_{i_l} \right) \quad (1)$$

where u_{i_l} denotes the normal velocity for the i_l th simple source on the l th layer interface and $\theta_{i_{l+1}, t}$ was the corresponding transmission angle (in layer $l + 1$). ρ_M and c_M are the density and sound speed respectively of the last layer (layer M). The complex acoustic wavenumber in the layer l is given by k_{c_l} , $R_{i_l, i_{l+1}}$ is the propagation distance from the i_l th simple source of area ds_{i_l} on the l th layer interface to the i_{l+1} th simple source of area $ds_{i_{l+1}}$ on the $(l + 1)$ th layer interface, the layer in between is layer l . The particle velocity transmission coefficient for the i_l th simple source on the l th layer interface can be written as:

$$T_{v_l} = \frac{2\rho_{l-1}c_{l-1}/\cos\theta_{i_l, i}}{(\rho_l c_l/\cos\theta_{i_l, t}) + (\rho_{l-1}c_{l-1}/\cos\theta_{i_l, i})} \frac{\cos\theta_{i_l, i}}{\cos\theta_{i_l, t}} \quad (2)$$

where the incidence and transmission angles $\theta_{i_l, i}$, $\theta_{i_l, t}$ satisfy Snell's law, i.e. $\sin\theta_{i_l, t}/\sin\theta_{i_l, i} = c_l/c_{l-1}$.

In the present case, the field was first propagated from a 15 cm radius hemispherical array onto the outer skull surface, then from the outer skull surface to the inner skull surface, and lastly from the inner skull surface into the brain tissue. The simulation algorithm was designed to allow the hemispherical surface to be divided into an arbitrary number of elements. The element phases were adjusted to maximize the pressure at the geometric centre of the hemisphere. Data for the simulation were obtained from a digitized human head profile obtained using MRI. A detailed description of the numerical algorithm is provided in the original work (Sun and Hynynen 1998).

2.2. Frequency optimization

Previous simulations (Sun and Hynynen 1999) indicate that the specific absorption ratio (SAR) and pressure gains between the ultrasound focus and the human skull are both at a maximum between 0.6 MHz and 0.7 MHz. That study was performed using data from a single human subject. The present study investigates gain considerations through direct measurement. Three formalin fixed *ex vivo* human skulls were used in the study. Acoustic properties of the fixed skulls were assumed to be similar to those of fresh skulls (Fry and Barger 1978). The experiment was designed to test the frequency dependence of ultrasound temperature and pressure gain. Measurements were made in a water tank using a focused broadband nine-element PZT 1–3 composite transducer array (Imasonic, France) as the signal source. The transducer has a diameter of 8 cm, a radius of curvature of 150 mm and a resonance of 0.9 MHz. Array elements are equal in area and consist of a central circular element surrounded by a ring sectioned into eight elements.

In order to maximize pressure, the phase of individual elements of the transducer was adjusted such that the acoustic waves from each element arrived at the geometric centre of the array with the same phase. After phase correction, a continuous-wave signal was applied for 80 s at a specific frequency. The procedure was repeated over the series of frequencies ranging from 0.5 MHz to 0.95 MHz at 0.05 MHz intervals. To reduce interference from standing waves between the transducer and skull surfaces, the skull was offset slightly from the transducer to reduce reflection back toward the transducer surface.

Over the 80 s sonication period, the acoustic pressure was monitored at the focus with a 0.5 mm diameter PVDF hydrophone (Precision Acoustics, UK). Simultaneously the temperature on the skull surface was recorded using a thermocouple placed on the skull in the approximate centre of the ultrasound beamwidth. Temperature data were read by an ISO Thermex thermocouple reader (Columbus Instruments, Ohio). After the thermocouple was placed on the skull surface it was covered by approximately 2 mm of a gel layer simulating skin (3M Kitecko, Minnesota). The procedure was repeated for three separate areas on a skull. Three calvaria were used in the experiment for a total of nine measured regions.

For absolute pressure measurement in the relevant frequency range, the PVDF hydrophone was calibrated between 0.5 MHz and 2 MHz in a water bath against a calibrated Marconi type Y-34-3598 membrane hydrophone in combination with a matched amplifier (GEC-Marconi, Essex, UK). This sensitivity was examined by sweeping the frequency over the relevant range as well as by pulsing the transducer and examining the output spectrum. Both methods gave similar results. A frequency-dependent calibration factor was obtained and applied to all hydrophone measurements.

To obtain a relative calculation of the power gain between the focus and the skull surface, the ratio of the square of the acoustic pressure at the focus to the change in surface temperature

$$G(f) = \frac{p(f)^2}{\Delta T(f)} \quad (3)$$

is considered where p is the acoustic pressure, ΔT is the change in temperature on the skull and f is the driving frequency. Both the pressure-squared values and the temperature change are quantities assumed to be directly proportional to the acoustic power. Temperature is monitored on the skull where acoustic properties are difficult to measure and pressure is measured after propagation through the skull where the phase of the propagating wave must be adjusted, as noted above, to restore the peak pressure at the geometric focus.

2.3. The 64-element hemispherical transducer

2.3.1. Construction. Based on the simulation study, a 64-element hemispherical array was constructed to demonstrate the feasibility of coagulating tissue volumes through a human skull. The array was constructed by cutting 64 single, 3.5 mm thick spherical segments with a diameter of 7 cm and a 15 cm radius of curvature into individually sized elements to form a hemispherical array. The elements were custom made from lead zirconate titanate (PZT-4) (Channel Industries, Santa Barbara, CA) electrically poled to operated in their thickness mode at a resonant frequency of 0.665 MHz.

As illustrated in figure 1, the curved elements are assembled to form a hemisphere with an inner radius of 15 cm. In order to transmit uniform power throughout the array, the elements were designed with a similar surface area ($\sim 22 \text{ cm}^2$) and element height ($\sim 5 \text{ cm}$). The result is an array consisting of a seven-sided polygonal top and four successive layers of quadrangular elements.

The gaps between elements are filled with silicone rubber to prevent water from entering the air-backed transducer as well as to provide mechanical and electrical isolation. Electrical

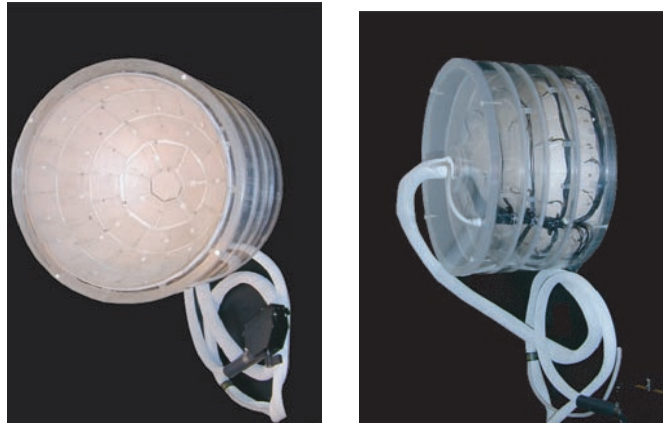


Figure 1. The trans-skull array.

contact to the transducer is attained by connecting the outer air-backed electrode with Belden 8700 coaxial cable. The inner face of the array is interconnected to a ground using soldered bridges of silver foil. The array is mounted in a sealed acrylic casing and the framework is given structural support by acrylic rings (figure 2) glued between each layer of elements.

2.3.2. Operation. Signals to the transducer are generated by a phased array driving system manufactured in-house similar to system reported by Daum *et al* (1998) but with a driving frequency range between 0.5 and 1 MHz. The amplifier is equipped with phase feedback for increased control. Individual array elements are matched to electrical resonance at 50Ω , to ensure maximum power output to the transducer. Electrical power supplied by the driving system is monitored by an internal power meter.

Transducer field measurements were conducted in a tank filled with degassed deionized water and padded with rubber to inhibit reflections from the tank walls. A 0.2 mm diameter polyvinylidene difluoride (PVDF) hydrophone (Precision Acoustics, UK) was positioned normal to the axis of symmetry of the array. The hydrophone was assumed to be omnidirectional at the driving frequency of 0.665 MHz. At this frequency the classical directional function for circular apertures (Pierce 1989) predicts the hydrophone response to change by less than -0.01 dB as a function of angle of incidence between 0° and 90° . The hydrophone was moved using a stepper-motor-controlled 3D positioning system (Parker Hannifin, Pennsylvania). The response of the hydrophone was sent through a Precision Acoustics preamplifier and recorded by a digital oscilloscope (Tektronix, Oregon, model 680). Both the scan position and the data acquisition are computer controlled. The hydrophone signal was downloaded to a PC and Fourier transformed to obtain the amplitude and phase of the resonant frequency. The acoustic amplitude as a function of position was obtained by placing the hydrophone at the geometrical centre of the hemisphere. The field was measured at 0.4 mm intervals over a $15 \times 15 \text{ mm}^2$ area.

Following measurement of the acoustic pressure field in water, a skull was placed between the hydrophone and the transducer and field was again recorded with all elements driven at the same amplitude and phase. Next, using feedback from the hydrophone, the phase of each element was manually adjusted to bring all elements in phase at the geometrical focus of the array. Another radial scan of the field was performed with the phase-corrected ultrasound.

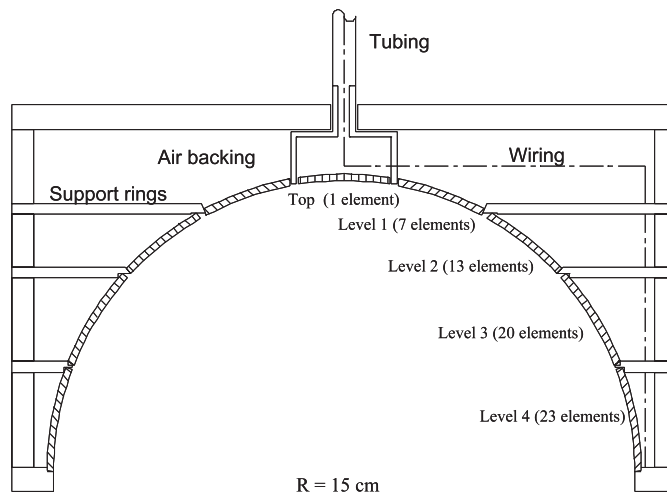


Figure 2. Cross section of the 64-element air-backed hemispherical array. Elements are approximately equal in area and have a resonant frequency of 0.665 MHz.

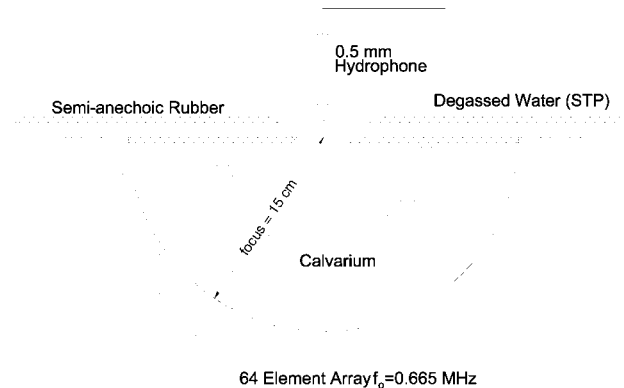


Figure 3. The experimental set-up used for phase measurements through human calvaria. Sound-absorbing rubber is placed directly on top of the hemispherical array. A stepper-motor-controlled positioning system guides the hydrophone.

As in the simulated case, the skull was also moved relative to the array in order to emulate mechanical shifting of the transducer. The skull was moved relative to its position in the initial trans-skull measurement. This shift was first performed along the axis of symmetry of the transducer and then in the radial direction normal to this axis. The field was measured over a series of positions along each shift direction. Before each measurement a new phase was determined for each element.

2.4. Thermal lesions

To demonstrate the feasibility of using the array for high-power therapeutic applications, thermally induced lesions were produced through the skull in tissue placed at the ultrasound focus. A focus was obtained through the skull by manual adjustment of the phase of each element at low power (<10 W electric power input to the transducer) as described in

section 2.3.2 and illustrated in figure 3. The amplitude of the driving signal was then increased to supply 41 W of electrical power to each element giving a total power of 2624 W supplied to the transducer. The ISO Thermex thermocouple reader monitors the temperature between the skull surface and a gel layer simulating skin (~ 2 mm of a 3M Kitecko ultrasound standoff pad) placed on the skull. It was decided to place the thermocouple at the interface between the synthetic skin and the surface of the skull bone because the highest temperature exposure to the skin occurs at this interface.

To test for lesions in fresh tissue, a thigh muscle from a sacrificed New Zealand white rabbit was removed and placed in a bag containing degassed 0.9% saline and heated to 37°C . The bag was attached to the Parker positioning system inserted into the skull immediately before powering the array. Sonications were performed in this manner at 8, 10 and 12 s.

3. Results

3.1. Frequency optimization

The normalized ratio between the pressure-squared measurement at the focus and the change in temperature on the skull surface is presented in figures 4(a)–4(c) showing measurements on each of the three skull samples. Peak gains range from 0.8 MHz (figure 4(a)) to below the lower measurement limit of 0.5 MHz (figure 4(c)). The optimal frequency is a function of the skull thickness, the lowest frequency occurring with the thickest skull. The mean gain for the combined nine measured skull regions is compared with a previously described theoretical value (Sun and Hynynen 1999) in figure 4(d). This theoretical value was obtained from thickness data using an MRI skull measurement of a single human head. The theoretical curve in the figure is observed to be broader than the experimental mean value with a peak gain at 0.6 MHz as opposed to the slightly higher experimental peak at 0.7 MHz.

3.2. Hemispherical array simulation

The radiating hemisphere was simulated after dividing it into 1, 8, 11, 64, 228 and 501 elements. The pressure about the geometrical centre of the array over a $15 \times 15 \text{ mm}^2$ area normal to the acoustic axis of propagation was calculated. For reference the Cartesian z -direction is defined along the hemisphere axis of symmetry. The driving frequency was 0.65 MHz and the total power over the hemisphere 1 W for each simulated case. At this frequency, the skull was assumed to possess a sound speed of 2652 m s^{-1} , a density of 1796 kg m^{-3} , and an attenuation coefficient of 60 Np m^{-1} . The brain tissue was assumed to have a sound speed of 1545 m s^{-1} , a density of 1030 kg m^{-3} and an attenuation of 2.6 Np m^{-1} (Sun and Hynynen 1999). The simulation of the field from a single-element focused hemisphere transducer in figure 5(a) may be compared with the squared values of the planar acoustic pressure amplitudes for 11, 64 and 501-element hemisphere arrays in figures 5(b)–5(d) after they are phase corrected to compensate for skull variation. Division of the transducer into an 11-element hemisphere, shown in figure 5(b), causes the scattered foci to converge onto a single peak at the geometric centre of the array. The pressure amplitude-squared values of slices of the fields through their foci are displayed in figure 6. It is noted that the full width at half maximum (FWHM) of the foci created by the 11- to 501-element arrays are similar ($\sim 0.9 \text{ mm}$) while peak values increase from $1.3 \times 10^{10} \text{ Pa}^2$ for 11 elements to $3.5 \times 10^{10} \text{ Pa}^2$ for 501 elements. Appreciable local maxima caused by diffraction remain in the region around the focus of the 11-element array. Further sectioning the array into 64 elements reveals decreased scattering away from the focus. Although the increase in maximum pressure continues as the hemisphere is further divided

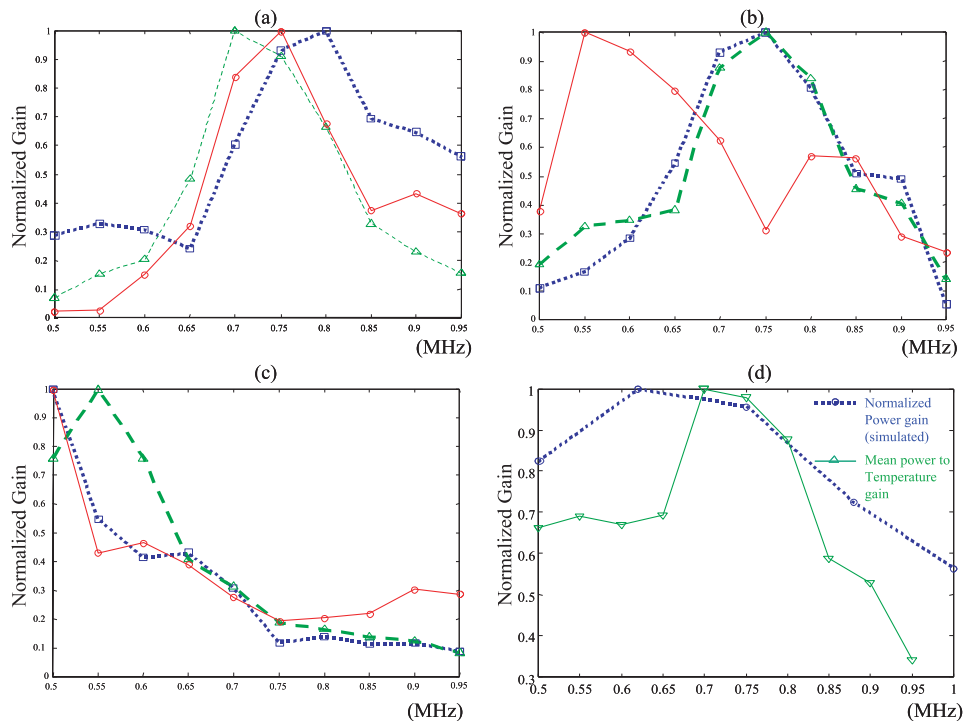


Figure 4. Normalized gain measurements displaying the ratio of the peak pressure at the focus through a human skull to the temperature rise on the skull surface: (a) Three separate regions measured on skull sample 1. (b) Measurements on sample 2. (c) Measurements on sample 3. (d) A comparison of the mean values of the above measurements with a simulated power gain measurement.

beyond 501 elements, there is a clear levelling of the slope at higher element numbers, as seen in figure 7, which plots the maximum pressure amplitude squared for each simulated array.

To model mechanical steering of the array, the hemisphere was shifted in its position relative to the skull and the pressure amplitude calculations repeated for the 64-element transducer with new phase corrections for each location. The first shift was 30 mm along the x -axis, normal to the axis of symmetry. The focus remained intact, although a slight drop in peak pressure was observed. Next, the array was moved to a position (20, 20, 20) mm along the Cartesian axes from its initial point relative to the skull. Figure 8 displays the resulting pressure field.

3.3. 64-element array

3.3.1. Ultrasound field measurements. The field produced by the 64-element array was measured in a plane about its geometrical focus after propagating through a human skull sample. The initial position of the focus was located at the approximate centre of the skull 7 cm from the midpoint of the sagittal suture. The pressure amplitude-squared plot about the origin is depicted in figure 9(a) with all elements driven in phase.

Next the focus was shifted along the transducer axis of symmetry by moving the skull away from the array. The elements were again phase corrected and the measurement repeated, converging the focus onto the geometric axis of symmetry shown in figure 9(b). Peak values

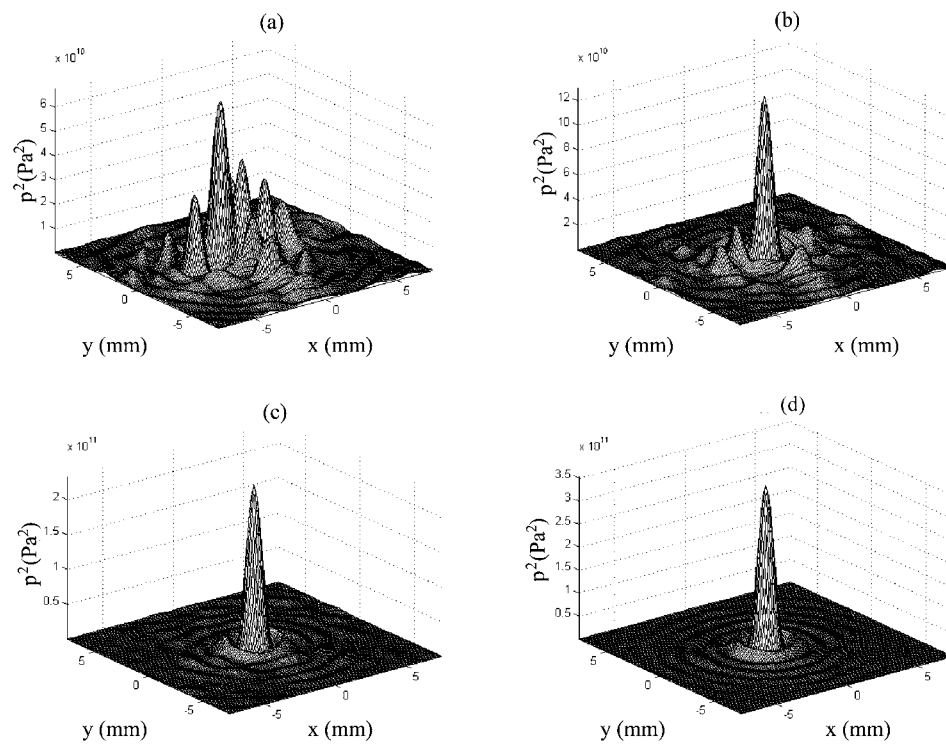


Figure 5. Pressure amplitude-squared field simulation of a hemispherical array focused through a human skull. The hemisphere is divided into (a) 1 element, (b) 11 elements, (c) 64-elements and (d) 501 elements.

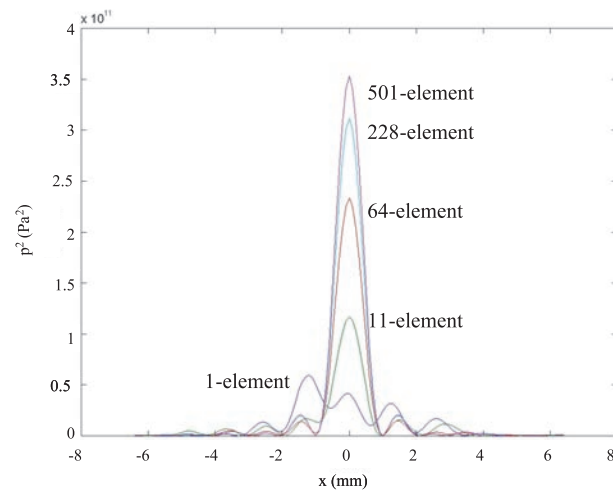


Figure 6. A radial cross section of the phase-corrected pressure amplitude-squared simulations for a radiating hemisphere divided into 1, 11, 64, 228 and 501 elements.

from the initial position to 30 mm were measured at 10 mm intervals. A drop in the focal peak is observed with each position as displayed by the square points in figure 10. Similarly the skull was moved in the radial direction relative to the transducer axis along a line roughly

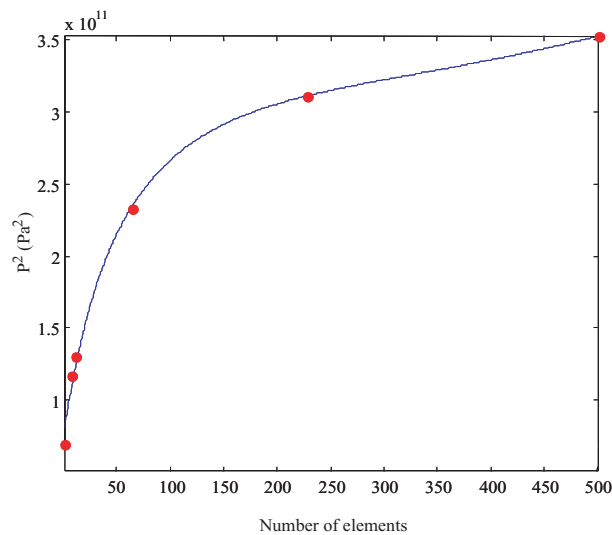


Figure 7. The maximum pressure-squared amplitude after trans-skull propagation as a function of the number of array elements.

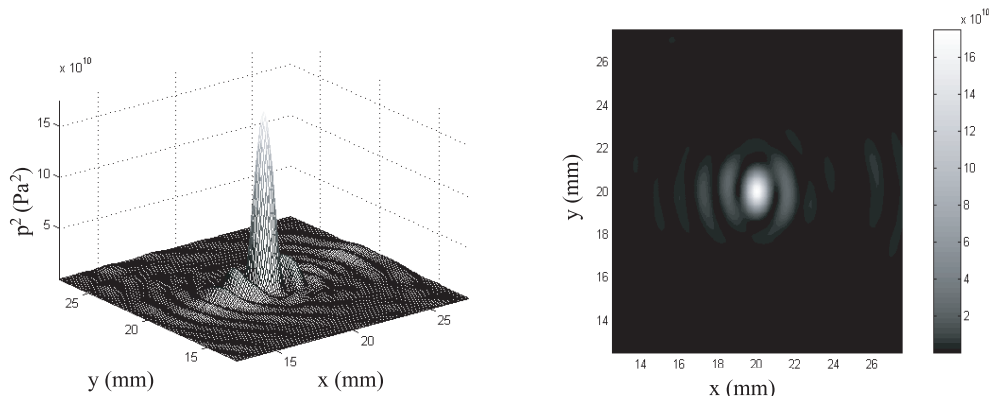


Figure 8. Simulated pressure amplitude-squared (left) and its contour (right) resulting from a shift of the transducer (20, 20, 20) mm relative to the skull.

normal to the sagittal suture. Circular points in figure 10 represent the measured peak pressure amplitude-squared as a function of distance. For comparison simulated results are also added to the plot. However, it is stressed that the simulation uses data from a different skull obtained from an *in vivo* MR measurement and a direct correspondence is not implied. The peak pressure amplitude-squared after a 30 mm axial shift was found to be 0.56 of the peak value at the originating position. When shifted in the direction perpendicular to the array, a 30 mm radial shift was measured at 0.52 of the centred skull value. In comparison, the simulation of this shifting (section 3.2) predicts a peak equal to 0.39 of its centred value after a 30 mm radial shift and 0.78 of its value after a 30 mm axial shift.

3.3.2. Lesions. Three lesions were created through the skull in rabbit tissue. The phased 2624 W signal was focused into the tissue for 8 s, 10 s and 12 s in different locations. A section of the lesion at 8 s as shown in figure 11 was sliced normal to the ultrasound axis at

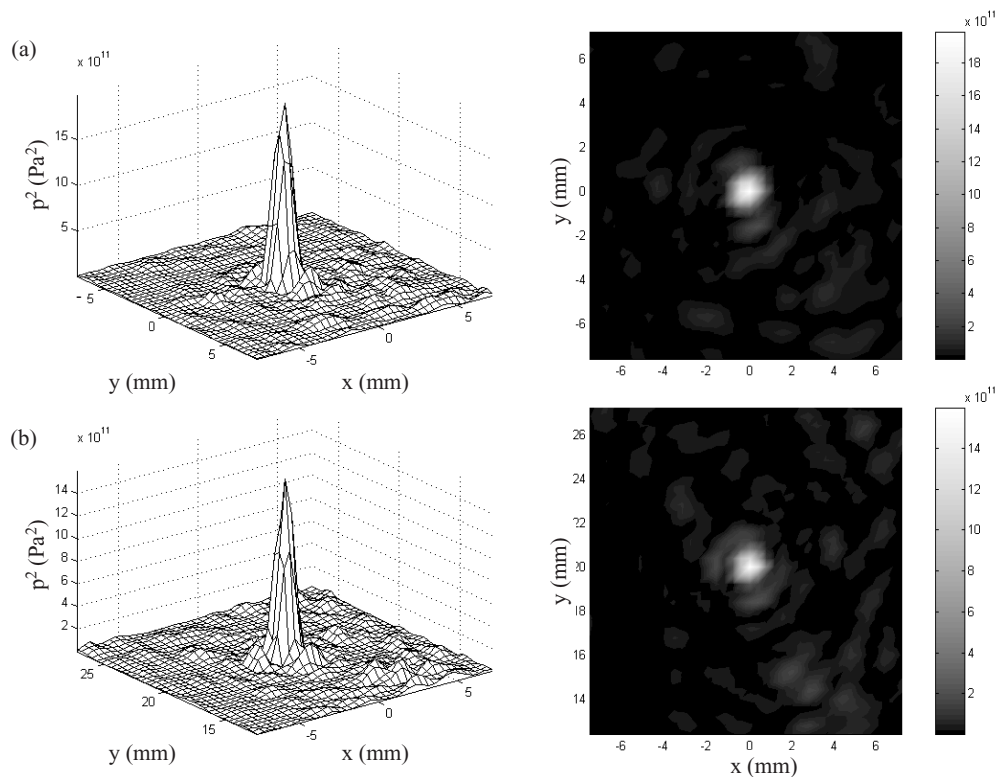


Figure 9. (a) Pressure amplitude measurement resulting from the 64-element array after all elements are phase corrected (left) and its corresponding contour plot (right). (b) Similar plots after the skull is moved 20 mm away from the array resulting in a focus closer to the skull surface.

the approximate centre of the lesion. Lesion dimensions were determined by visual inspection and measured radially along two orthogonal axes and along the lesion axis. The lesions were found to be nearly spherical in shape and range in size from a diameter and length of $D_{\max} = 6.5$ mm, $L_{\max} = 7.5$ mm for a 12 s sonication, $D_{\max} = 6.5$ mm, $L_{\max} = 7.5$ mm for a 10 s sonication and $D_{\max} = 1.7$ mm, $L_{\max} = 2.0$ mm for an 8 s sonication. Changes in skull surface temperature ranged from 12.4 °C to 18.6 °C. The lesions were found to be reproducible in subsequent sonications.

4. Discussion

This study confirms our previous study with virtual array experiments (Clement *et al* 2000), showing that a hemispherical array can focus through the human skull. The high-power experiments demonstrate for the first time that this focus is sufficient to coagulate tissue without cutaneous burning of the skin across the scalp (Moritz and Henriques 1947). These results are significant, demonstrating that practical and completely non-invasive ultrasound surgery is possible and that it can be done with a relatively small number of phased array elements. The results open the way for the development of clinical phased array systems.

A resonant frequency near 0.7 MHz was chosen for the array using numerical and experimental thermal gain measurements between the transducer focus and the skull.

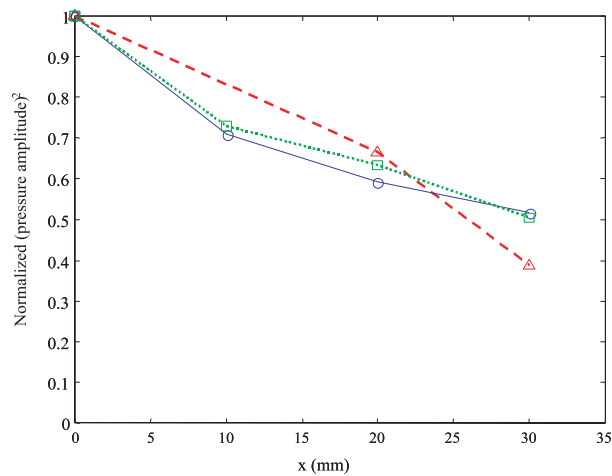


Figure 10. Peak pressure amplitude-squared values after phase-corrected transcranial propagation as a function of focal location within the skull. Starting from an origin located at the approximate centre of the skull, the skull is moved away from the transducer (squares) and normal to the transducer (circles). These measurements are compared with the simulated case (triangles).

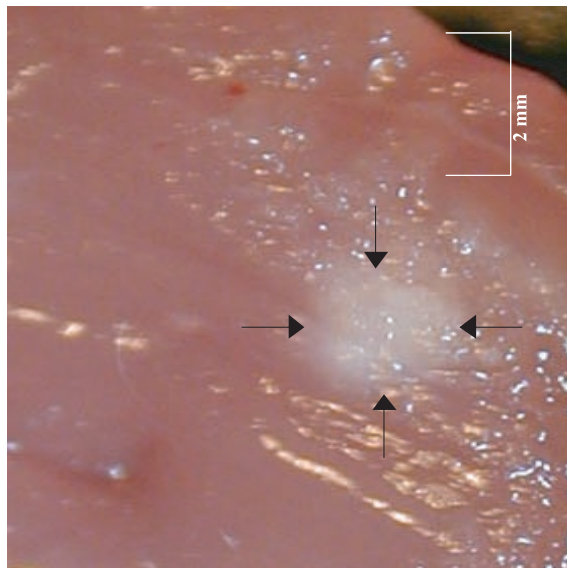


Figure 11. Lesion produced in *ex vivo* rabbit thigh muscle placed inside a human skull using an 8 s sonication at 2624 W.

Experimental determination of optimal driving frequencies was achieved by comparing field measurements at the focus through the skull with temperature measurements on the skull surface. Frequency-gain dependence was controlled primarily by two factors: focal size and the attenuation coefficient of the skull. That is, a higher frequency can achieve a more localized focus but will have a higher fraction of its energy absorbed by the skull. Consequently the frequency must balance the effects of attenuation with focal size. Experiments give an indication of the ratio of the pressure-squared value at the focus to the temperature rise on

the skull surface. Peaks are found to range from below the measurement limit of 0.5 MHz up to 0.8 MHz, being a function of skull thickness with the lowest limit occurring with the thickest skull. Additionally, variation is observed at different locations on the same skull. This indicates that the optimal treatment frequency may be different for each patient.

Simulations provide information on the improvement of the acoustic field from a hemispherical radiator as it is divided into an increasing number of elements. For the physical transducer this number must be large enough to provide a focus capable of producing a thermally induced lesion without excess heating outside the treatment area. At the same time, the number of elements should be minimized to simplify the procedure and lower the cost of the total system, making it more practical. Dividing a hemisphere radiator into phased equal-area elements predicts that the peak acoustic pressure will approach a limiting value as the number of elements is increased (figure 7). A 64-element design was chosen for the array due to its ability to reconstruct the focus through the skull without a prohibitively large number of elements. The 64-element array simulation, shown in figure 9(b), reconstructs the focus through the skull centred about the array in addition to producing a peak pressure amplitude-squared 1.9 times larger than the 11-element simulation. A further increase in the number of elements extends the focal gain to 5.2 with a 500-element array. However, the simulation indicates that the 64-element design should be adequate to demonstrate the feasibility of this approach.

Further simulation (figure 8) shows the ability of the 64-element array to shift a distance of (20, 20, 20) mm relative to the skull and still produce a focus. Shifting of the skull relative to the geometric focus was also studied experimentally using the 64-element hemispherical array. Similar to the simulated case, measurement after shifting found that the focus remained intact but with a lower amplitude (figure 9(b)). Results shown in figure 10 indicate that this design of array should be able to treat target volumes within a cube of $60 \times 60 \times 30 \text{ mm}^3$ in the centre of the brain, assuming the effective volume is within 50% of the peak pressure-squared value. This is consistent with the results of earlier simulations (Sun and Hynynen 1999).

The 64-element array produced trans-skull pressure amplitude-squared focal peaks that were on average 10% of the peaks measured in water without a skull. For comparison an ideal case was considered. Assuming a power transmission coefficient of 0.53 incident through the skull and an absorption of 60 Np m^{-1} throughout a uniform 7 mm skull, the maximum expected pressure amplitude-squared is 0.22 of the value without the skull assuming normal incidence upon the inner and outer surfaces. Examination of figure 7 shows the 64-element array to be approximately 0.6 the value of convergence limit of the hemisphere as the number of elements grows toward a continuous case. In this situation a pressure amplitude-squared peak equal to 14% of the peak in water without a skull would be expected.

Functionality of the array is demonstrated by producing lesions in tissue after properly phasing the array and propagating ultrasound through an *ex vivo* human skull. Lesions ranged from 1.5 mm to 7.5 mm in diameter. In practice large volumes could be treated using mechanical shifting of the array to produce a succession of small lesions. Temperature measurements on the skull surface during production of lesions ranged from 12.4 °C to 18.6 °C above the ambient water temperature of approximately 21 °C. This peak temperature rise during the 8–12 s sonication is acceptable if surface cooling is used to reduce the temperature of the skin–bone interface before sonication. In addition, this measurement is most probably higher than would be encountered in an *in vivo* measurement as the artificial skin was thicker than actual skin and there was no cooling due to blood perfusion.

Although 64 elements are sufficient for producing lesions, we note that additional elements would increase the power delivered to the focus (figure 6) and thus reduce the increase in temperature at the bone surface. The advantage of increasing the number of elements approaches a limit, as seen in figure 7, which indicates the increase in peak power rapidly

approaching a limiting value. Little improvement at the geometrical focus is expected beyond division of the hemisphere into 500 elements. However, further division into even smaller elements could increase the range for electronic beam steering. For the 64-element array accurate placement of the focus could be accomplished by a precision positioning system that would mechanically shift the array. An array with more elements could also control the focal position electronically. Patient treatment could use the array with a phase prediction model to determine the driving phases of individual elements (Hynynen and Sun 1988) along with MRI to monitor treatment progress (Hynynen *et al* 1996), resulting in a fully non-invasive procedure. Although clinical implementation of this non-invasive focused ultrasound brain surgery still requires more basic work, the current study demonstrates its feasibility and proposes a practical design for such a clinical method.

References

- Clement G T, White J P and Hynynen K 2000 Investigation of a large area phased array for focused ultrasound surgery through the skull *Phys. Med. Biol.* **45** 1071–83
- Daum D R, Buchanan M T, Fjield T and Hynynen K 1998 Design and evaluation of a feedback based phased array system for ultrasound surgery *IEEE Trans. Ultrason. Ferroelectr. Freq. Control* **45** 431–4
- Fry F J 1977 Transkull transmission of an intense focused ultrasonic beam *Ultrasound. Med. Biol.* **3** 179–84
- Fry F J and Barger J E 1978 Acoustical properties of the human skull *J. Acoust. Soc. Am.* **63** 1576–90
- Fry F J and Goss S A 1980 Further studies of the transkull transmission of an intense focused ultrasonic beam: lesion production at 500 kHz *Ultrasound. Med. Biol.* **6** 33–8
- Fry F J, Sanghvi N T, Morris R F, Smithson S, Atkinson L, Dines K, Franklin T and Hastings J 1986 A focused ultrasound system for tissue volume ablation in deep seated brain sites *IEEE 1986 Ultrasonics Symp. Proc.* (IEEE) pp 1001–4
- Hynynen K, Freund W R, Cline H E, Chung A H, Watkins R D, Vetro J P and Jolesz F A 1996 A clinical non-invasive MRI monitored ultrasound surgery method *RadioGraphics* **16** 185–95
- Hynynen K and Jolesz F A 1998 Demonstration of potential non-invasive ultrasound brain therapy through an intact skull *Ultrasound. Med. Biol.* **24** 275–83
- Hynynen K, Vykhodtseva N I, Chung A H, Sorrentino V, Colucci V and Jolesz F A 1997 Thermal effects of focused ultrasound on the brain: determination with MR imaging *Radiology* **204** 247–53
- Moritz A R and Henriques F C 1947 The relative importance of time and surface temperature in the causation of cutaneous burns *Am. J. Pathol.* **23** 695–721
- Pierce A D 1989 *Acoustics, An Introduction to Its Physical Principles and Applications* (Woodbury, NY: Acoustical Society of America)
- Robinson T C and Lele P P 1972 An analysis of lesion development in the brain and in plastics by high-intensity focused ultrasound at low-megahertz frequencies *J. Acoust. Soc. Am.* **51** 1333–51
- Sun J and Hynynen K 1998 Focusing of therapeutic ultrasound through a human skull: a numerical study *J. Acoust. Soc. Am.* **104** 1705–15
- 1999 The potential of trans-skull ultrasound therapy and surgery using the maximum available skull surface area *J. Acoust. Soc. Am.* **105** 2519–27
- Tanter M, Thomas J-L and Fink M A 1998 Focusing and steering through absorbing and aberrating layers: application to ultrasonic propagation through the skull *J. Acoust. Soc. Am.* **103** 2403–10